DOE/ER/14179--2

DE93 006423

Stability and heat transfer in time–modulated flows
Technical Progress Report: DOE/ER/14179–2

C. Thompson

Department of Electrical Engineering
Laboratory for Advanced Computation
University of Massachusetts–Lowell
Lowell, MA 01854

DISCLAIMER

This report was prepared as an account of work sponsored by an agency of the United States Government. Neither the United States Government nor any agency thereof, nor any of their employees, makes any warranty, express or implied, or assumes any legal liability or responsibility for the accuracy, completeness, or usefulness of any information, apparatus, product, or process disclosed, or represents that its use would not infringe privately owned rights. Reference herein to any specific commercial product, process, or service by trade name, trademark, manufacturer, or otherwise does not necessarily constitute or imply its endorsement, recommendation, or favoring by the United States Government or any agency thereof. The views and opinions of authors expressed herein do not necessarily state or reflect those of the United States Government or any agency thereof.

MASTER

DISTRIBUTION OF THIS DOCUMENT IS UNLIMITED

Stability and heat transfer in time–modulated flows
Technical Progress Report: DOE/ER/14179–2

C. Thompson

Department of Electrical Engineering, Laboratory for Advanced Computation
University of Massachusetts–Lowell, Lowell, MA 01854

The report outlines research activities currently underway in the Laboratory for Advanced Computation at the University of Massachusetts–Lowell under DOE grant DE–FG02–91ER14179. A summary of results for the period November 1991 to November 1992 conducted under the program is given.

Table of Contents

Abstract 1

Table of Contents 2

1.0 Introduction 3

2.0 Technical Results 6
- 2.1 Chaotic secondary motion in oscillatory boundary layers 6
- 2.2 Space–time evolution of unstable disturbances in a Stokes boundary layer 8
- 2.3 Characterization of the velocity in chaotic unsteady flows 14
- 2.4 Ultrasonic characterization of vortical structures 19
- 2.5 Construction and evaluation of the experiment 20

References 27

1.0 Introduction

In May 1991, DOE awarded grant DE–FG02–91ER14179 for the investigation of stability and heat transfer in time–modulated flows. This investigation involves modeling and characterization of unstable oscillations in a two dimensional oscillatory boundary layer.

The basic flow considered is a modification to the solution of Stokes's second problem. In the problem as formulated by Stokes [1] and Rayleigh [2], the fluid adjacent to a rigid planar surface is driven into motion by a time–harmonic in plane displacement of the surface. Modified problems usually involve consideration of the type of forcing and the surface geometry. In wall bounded flows, the oscillatory motion is the result of an externally applied pressure gradient. Deceleration of the fluid at rigid boundaries results in the formation of a viscous boundary layer adjacent to the surface. This layer is called the Stokes boundary layer.

For planar surfaces, stability analyses have concluded that the Stokes boundary layer is linearly stable to two and three–dimensional vortical disturbances [3] [4]. This body of work is based on the hypothesis that the Stokes boundary layer becomes unstable at a threshold value of

the streaming Reynolds number R_s. The streaming Reynolds number R_s being defined as $U_\infty^2/(\omega\nu)$, where ν is the kinematic viscosity of the fluid. The variables ω and U_∞ represent the frequency and velocity amplitude of the excitation respectively. Thus far all have concluded that the Stokes boundary layer is stable to disturbances having infinitesimal amplitude. The absence of a bifurcation point according to linear theory has motivated investigators to look at the effects of finite amplitude disturbances on the stability of the Stokes boundary layer. Recently Akahavan *et al*[4] concluded that instability of the secondary flow, generated by finite amplitude linearly stable two–dimensional perturbations, may be responsible for transition to turbulence.

In the allied problem of a Stokes boundary layer generated by the transverse oscillation of a cylinder, Hall[5] theoretically obtained a bifurcation point according to linear theory. This instability had been earlier observed experimentally by Honji[6] and corroborated by Sarpkaya[7]. It was found that convex curvature of the boundary gives rise to centrifugal destabilization of the Stokes boundary layer. The relationship between the boundary geometry and modulation amplitude has been investigated

by Thompson *et al* [8] [9] [10]. This work has shown that the stability of the Stokes boundary layer is a function of three nondimensional parameters ϵ, R and R_s. The parameter ϵ represents the slope of the boundary. The oscillatory Reynolds number R is defined as $(\omega H_o^2/\nu)^{1/2}$, where the length scale H_o is taken to be the magnitude of channel's height variation. In channels having a slowly varying cross section, a viscous streaming flow occurs for low amplitude excitation. For small values of $\epsilon^2 R_s$ there is little interaction between the viscous streaming and basic flows. As the excitation amplitude is increased, instability occurs. For a finite value of the curvature ϵ^2, three dimensional vortical disturbances bifurcate from stability at T^2 equal to 16.92, where T^2 is equal $\epsilon^2 R_s/R^{1/2}$. More over if T is further increased temporal chaos ensues. Therefore, when boundary curvature is present, the Stokes boundary layer losses stability at a finite amplitude.

During the November 1991–1992 period, the emphasis of the research has been placed on theoretical and experimental models of modulational instability. In addition sensitivity of modulational instability to spectral content of the perturbing disturbance has been investigated.

2.0 Technical Results

2.1 Chaotic secondary motion in oscillatory boundary layers

As the Taylor number T increases, the two dimensional oscillatory flow in channel having walls with convex curvature undergoes subcritical transition from 2−D Stokes boundary layer to a state where streamwise oriented vortices appear. The temporal growth in amplitude of these streamwise vortices is the result of the imbalance between the centrifugal force and the pressure. The most unstable axial position along the channel corresponds to the location where the convex wall curvature is maximum. For a fixed value of the curvature, instability ensues above the critical value T_c. These periodic vortices have a spanwise wavenumber of κ_c. At T_c there is only one linearly unstable wavenumber. As the Taylor number is increased beyond T_c a continuous range of spanwise wavenumbers are unstable. According to linear theory, the most unstable of these wavenumbers remains κ_c. From this view point the dominance of the least stable or primary mode should persist through amplitude saturation.

In any practical situation, the initial spatial wavenumber spectrum is comprised of super and subharmonics κ_c. In such a case the growth and long−time behavior of the flow is mediated by the energy balance between these modes. Some preliminary results describing the effect of the spatial wavenumber content of the disturbance on Stokes boundary layer has recently been presented by Thompson *et al.* [11] [12]. The objective of this work was to ascertain how sensitive the primary flow is to secondary disturbances. At low amplitudes these secondary disturbances, according to linear theory, would be stable or have a slow growth rate when compared to the primary disturbance. The objective of this work was to 1)determine if the primary mode is dominant under broad−excitation, 2) identify spatial bifurcations and detuning of the least stable wavenumber for increasing Taylor number and 3)determine the relationship between spatial and temporal bifurcations. To this end, secondary disturbances having subharmonic spanwise spatial harmonics were considered.

The energetics and structure of the velocity field in the presence of Fourier modes having integral multiples of $\kappa_c/4$ was examined. The initial energy amplitude of each Fourier mode was set to an equal value.

The growth in the energy amplitude of each mode was recorded for increasing time. As time increases, each of these Fourier modes may be considered as samples of the wavenumber spectrum.

It was found [13] that the presence of subharmonics delayed the onset of chaotic oscillations only slightly. However, we found that nonlinearity affords detuning for the least stable wavenumber κ_c. We have observed that as T was increased above the critical value the unstable streamwise oriented vortices had a wavenumber of $3\kappa_c/4$ rather than the value κ_c predicted by linear theory. In addition, as T is further increased, the Fourier mode having $\kappa_c/2$ is dominant. The detuning of the Fourier mode having the maximal response is in qualitative agreement with observations of Honji [6] for the problem of flow instability of the Stokes boundary for a harmonically oscillating circular cylinder.

2.2 Space–time evolution of unstable disturbances in a Stokes boundary layer

In previous work, a local analysis valid near the point of maximum convex curvature was used. Such analyses have been helpful in identifying

the basic instability mechanism and characteristics in the Stokes layer problem. For a comprehensive description of the transition process the development of a model that incorporates the axial variations in the basic and unstable flow is necessary.

The stability of oscillatory flow in a channel having a gaussian variation in height $h(x)$ described by

$$h(x) = e^{-\epsilon^2 x^2/2}$$

has been examined. In this work the local value of the Taylor number varies as

$$T^2(x) = T_o^2 \left(1-\epsilon^2 x^2 \right) h(x) u^2(x)$$

where T_o is the Taylor number at x equal to zero and $u(x)$ is the amplitude of the axial component of the freestream particle velocity normalized by its value at x equal to zero. For a disturbance having a finite amplitude the threshold of instability occurs at T^2 equal to 10. Using this result, we find that instability occurs only in the region

$$-\left(1-10/T_o^2\right)^{1/2} < x\epsilon < \left(1-10/T_o^2\right)^{1/2}$$

For high enough values of T_o the flow can exhibit bistable oscillations at the edges of the region while semiperiodic and chaotic oscillations occur at the interior. To properly resolve such axial variations in the velocity a hybrid spectral and B−spline based numerical algorithm has been developed. In the axial direction B−spline basis functions were chosen because of their local support and high accuracy. The vertical and span-wise decomposition was done using Chebyshev polynomials and Fourier series respectively.

The resulting system of equations is rather unwieldy. However, significant progress has been made in optimizing portions of this code. This process has resulted in six fold speed increase and half the memory requirement of earlier realizations. Preliminary results of these calculation have been presented at national meetings of the Acoustical Society of America[14] and the American Physical Society[15].

For R equal to 10^4, it was found that the unstable disturbances are either periodic or semiperiodic for T_o below $(85)^{1/2}$ for a disturbance field

comprised of the spanwise Fourier mode κ_c and four of its integral multiples. This disturbance field begins to exhibit chaotic oscillations at T_o equal to $(85)^{1/2}$. An examination of the modal kinetic energies show that the κ_c mode dominates. The energy amplitude for increasing integral multiples of κ_c decays exponentially; the ratio between the energy amplitudes of the κ_c and $5\kappa_c$ modes is $O(10^{-4})$. The rapid decay in the modal energies is taken as justification for truncating the Fourier series at six modes. The structure of the disturbance velocity field for one period of oscillation is illustrated in Fig. 2.2.1 by flow vectors. The velocity in the $x-y$ section at $z = 0$ is shown in Fig. 2.2.1(a), and a $z-y$ section at $x = 0$ is shown in Fig. 2.2.1(b). A single vortex spans the $z-y$ cross-section, whose dimensions are $\pi/(\kappa_c)$ along z and 20 boundary layer units along y. Although, a second vortex does intermittently appear. The vortices appear distorted, that is, they are not symmetric about the line $z = \pi/(2\kappa_c)$. A connection between the loss of spanwise symmetry and temporally chaotic behavior is not clear since some asymmetry in the spanwise vortices is present even for values of T_o for which the temporal behavior is periodic. The $x-y$ cross-section reveals that the streamwise

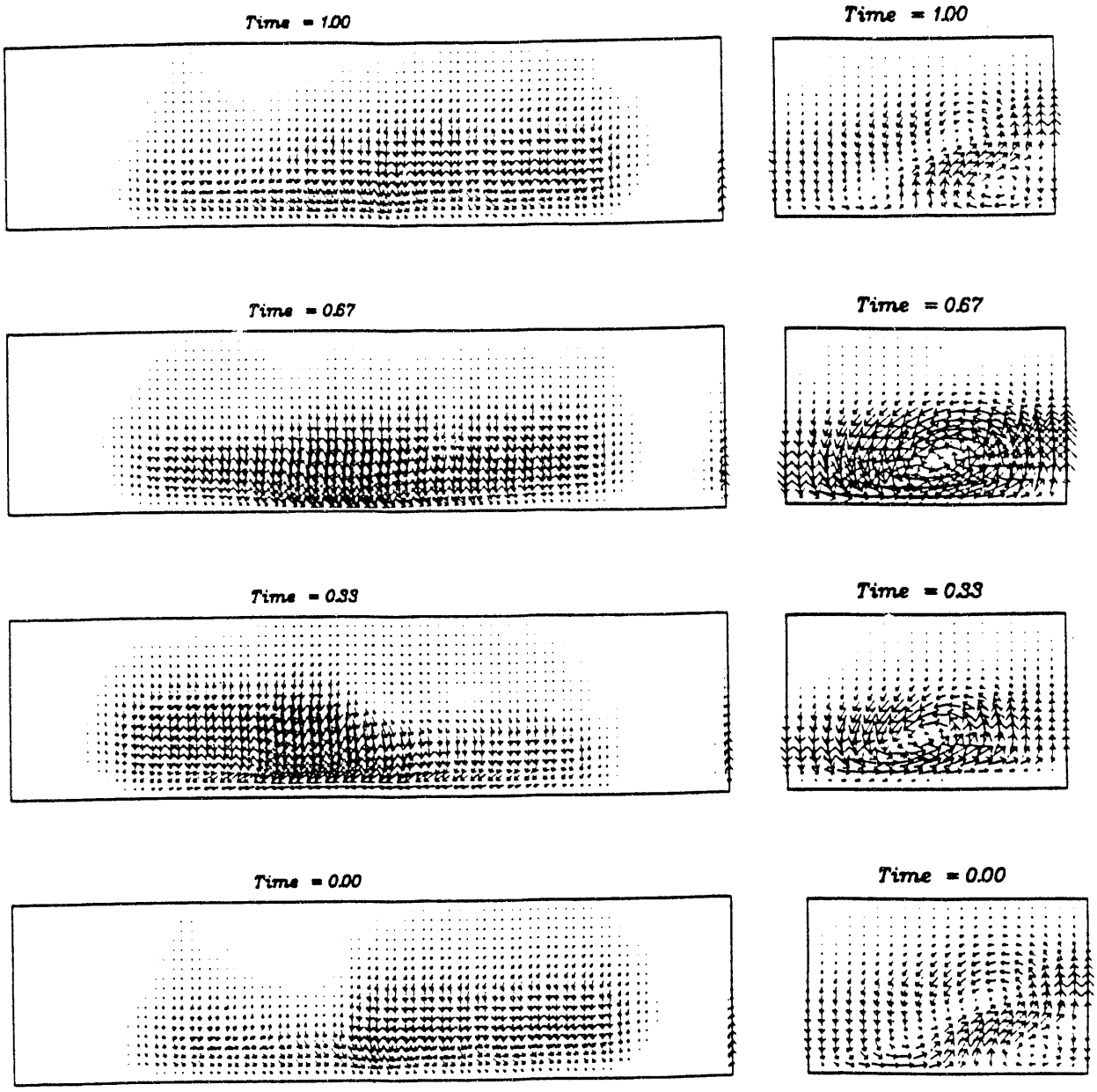

(a) x − y section at z = 0

(b) z − y section at x = 0

Figure 2.2.1 Velocity vectors over one period for $T_* = (85)^{1/2}$

component of the disturbance velocity is weak in comparison to the vertical and spanwise components. The flow vectors show a streamwise vortex with a positive streamwise vorticity component. The vortex appears to be of finite length along the streamwise coordinate, i.e. the disturbance velocity is found to decay rapidly beyond a certain streamwise position $|x| > x_c$. This behavior is consistent with the change in the local value of T along the streamwise coordinate due to a change in the boundary curvature. If we predict the local value of T by making a rough estimate of x_c from the flow vector plot, we find that the cutoff value of the Taylor number $T(x_c)$ falls between $(10)^{1/2}$ and $(17)^{1/2}$ for all cases investigated.

In the case where the disturbance field is composed of the mode $\kappa_c/4$ and four of its integral multiples, results indicate a non-linear detuning in the spanwise wavenumber. For $T_o = (25)^{1/2}$ the kinetic energy in the $3\kappa_c/4$ mode is dominant. This result is supported by the experimental observations of Honji[6]. In fact, we find that, for an initial disturbance field consisting of modes with comparable kinetic energies, only the $3/4\kappa_c$ mode reaches an equilibrium energy amplitude. The remaining modes experience a short period of growth followed by

unabated decay. We note that this subharmonic mode saturates for an energy level greater, by a factor of 10, than that for the $T_o = (85)^{1/2}$ case mentioned above. Local analysis performed by Mulpur *et.al* [13] have found that subharmonic spanwise modes generally allow for higher saturation energies than superharmonic modes for fixed T_o. Since results show wavenumber detuning while the time behavior is still periodic, we expect spatial bifurcations to be independent of temporal bifurcations. The disturbance velocity field for this case is composed of spanwise vortices of wavelength $(8\pi)/3\kappa_c$. These vortices are localized to a region x:[$-x_c$, x_c], such that $T(x_c) = (11)^{1/2}$.

2.3 Characterization of the velocity in chaotic unsteady flows

In the numerical model, axial variations in velocity amplitude are expressed in terms of B−splines having local support. The disadvantage of this representation is the large number of functions required. An orthogonal decomposition of the velocity was carried out to determine if an optimal set of basis could be obtained. Traditionally, this is done by

applying the Karhunen–Loeve expansion on the time–averaged two–point spatial correlation of the velocity [16]. The use of the time–averaged velocities is justified when the underlying process is ergodic. The chaotic flows investigated here do not satisfy this requirement.

The vector velocity coefficient of the $n-th$ spanwise Fourier mode is $\underline{u}^n$.

$$\underline{u}^n = \sum_{i=1}^{M} \sum_{j=1}^{K} \underline{U}_{ij}(t)\ T_j(y)\ B_i(x)$$

The variation in the y direction is represented by Chebyshev polynomials of the second kind T_j and B_i represents the B–spline basis. In a typical calculation K is equal to eight and M is equal to forty.

The dominant velocity components are identified by examining the ensemble mean and variance of the Fourier coefficients as a function of time. The vertical velocity components of the first three Fourier modes were found to dominate the velocity field. The axial variation of the y–averaged vertical velocity of the first Fourier harmonic $<v^1>$ is shown in Figs. 2.3.1. In these figures constant amplitude contours are plotted as a

function of x and time. Figs. 2.3.1(a) and (b) represent the periodic oscillations that occur at T^2 equal to 50 and the chaotic oscillations that occur at T^2 equal to 85 respectively. The horizontal axis represents the axial distance and the vertical axis represents time.

The determination of the optimal set of modes necessary to represent the flow was carried out by first constructing the average spatial waveform for each velocity component. Samples of the waveform having the same time−phase relative to the excitation were averaged over successive periods [17]. This determines the ensemble mean value of the velocity component at each spatial location. The length of the ensemble is taken to be one cycle of the excitation signal. This overcomes the problem of the nonstationarity of the ensemble. Typically 60 time samples per period of the excitation are used. The spatial correlation matrix $R(x,x',t)$ of the averaged waveform was then computed for each time sample. The orthogonal modes obtained from the Karhunen−Loeve decomposition allow the optimal representation for the spatial velocity variations at each time sample. Under the constraint that the coefficients $\underline{U}_{ij}$ are delta correlated, the optimal N number of modes ϕ_n can be shown to be the normal-

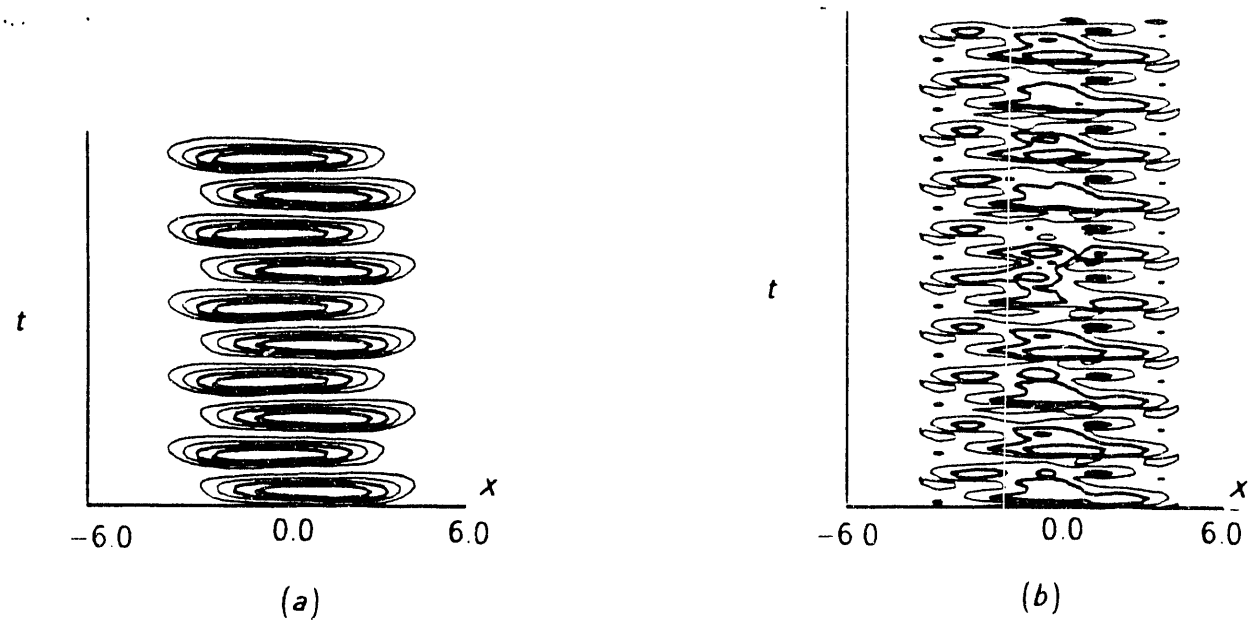

Fig. 2.3.1 : Constant contour plots of the axial variation of y averaged vertical velocity $<v^1(t)>$. Vertical axis represents time samples. (a) Periodic oscillations for $T^2=50$. (b) Chaotic oscillations for $T^2=85$.

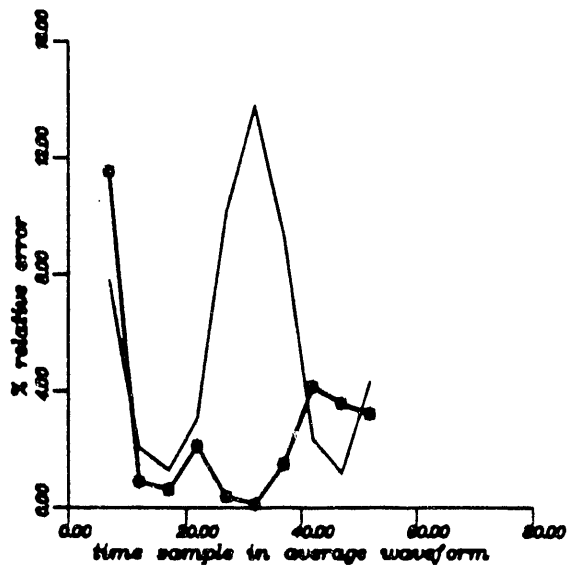

Fig. 2.3.2 : Comparison of the percentage relative error between reconstructed and original energy of $<v^1(t)>$ for ensemble averaged waveform of the chaotic case in Fig. 2.3.1(b). Solid line depicts reconstruction under assumption of stationarity. Symbols depict reduction in error when basis functions were computed for all time signatures.

ized eigenvectors of $R(x,x',t)$. The super set of the functions ϕ_n is obtained from the union of all of the realizations from each time sample. This combination of functions can form a linearly dependent set. The redundant functions are eliminated by using the Gram−Schmidt orthogonalization process. The result of this process is the minimal basis set that satisfactorily accounts for 90% of the signal energy content. Typically for the case where T^2 equals 85, fifteen basis functions were found to be optimal. This allows B_i to be replaced by the new set of functions ϕ_i.

The Karhunen−Loeve basis do not satisfy the boundary conditions. Therefore, linear combinations of these functions were used when required. Fig. 2.3.2 shows the relative percentage error between the reconstructed and the actual energy of $<v^1>$ versus time. These results are for the chaotic case of T^2 equal to 85. The solid curve shows the result when the basis functions were obtained under the assumption that $<v^1>$ was statistically stationary. The time signatures used to derive the basis set under the stationary assumption, were those that exhibited the highest mean and variance in time. The symbols in Fig. (2.3.2) represent the error when the optimal basis was the super set of the Gram−Schmidt

process which was applied to the functions obtained from all of the time signatures in the average waveform. The relative error is within 10% except at the first peak, which corresponds to a signal whose energy is at the noise floor of the calculation.

2.4 Ultrasonic characterization of vortical structures

Vortical fluid structures in low mach number flows have been shown to be responsible for radiation and scattering of sound [18] [19]. This study is aimed at the quantitative characterization of the vortical disturbances, by measurements of the scattered sound. The drawback in previous theories is the neglect of the interference between the sound scattered by different regions of the flow. This first order scattering theory has been recently improved [20] to allow the computation of higher order effects. Information on the spatial distribution of the disturbances can be determined when acoustic wavelengths are comparable to the vortex size. The theoretical framework for analyzing the scattering problem at these scales as well as methods for extracting the pertinent features of the flow field have been developed. Simulations of acoustic wave propagation and

scattering from vortical disturbances show that the spatial wavenumber content of the velocity perturbations can be determined from far field observations of the scattered field [21].

2.5 Construction and evaluation of the experiment

Preliminary experiments on instability in the Stokes boundary layer are being carried out using a rectangular channel with a single open end. See Figure 2.5.1. The channel is 3.81 *m* in length and its cross section has dimensions 38 *cm.* *x* 21 *cm.* The channel is constructed from 3/4 *in.* plywood. The interior walls are covered with formica to provide a smooth surface. The lower boundary varies in height in the axial direction with the maximum elevation being $10cm$. The maximum nondimensional curvature ϵ^2 is $(0.2)^2$.

The lower boundary shape is realized by overlaying a sheet of formica on top of a shaped frame. The formica skin is supported and stiffened by spanwise ribs. The skin is held in place by contact cement and the ribs are fastened at the ends to two gaussian shaped plywood panels.

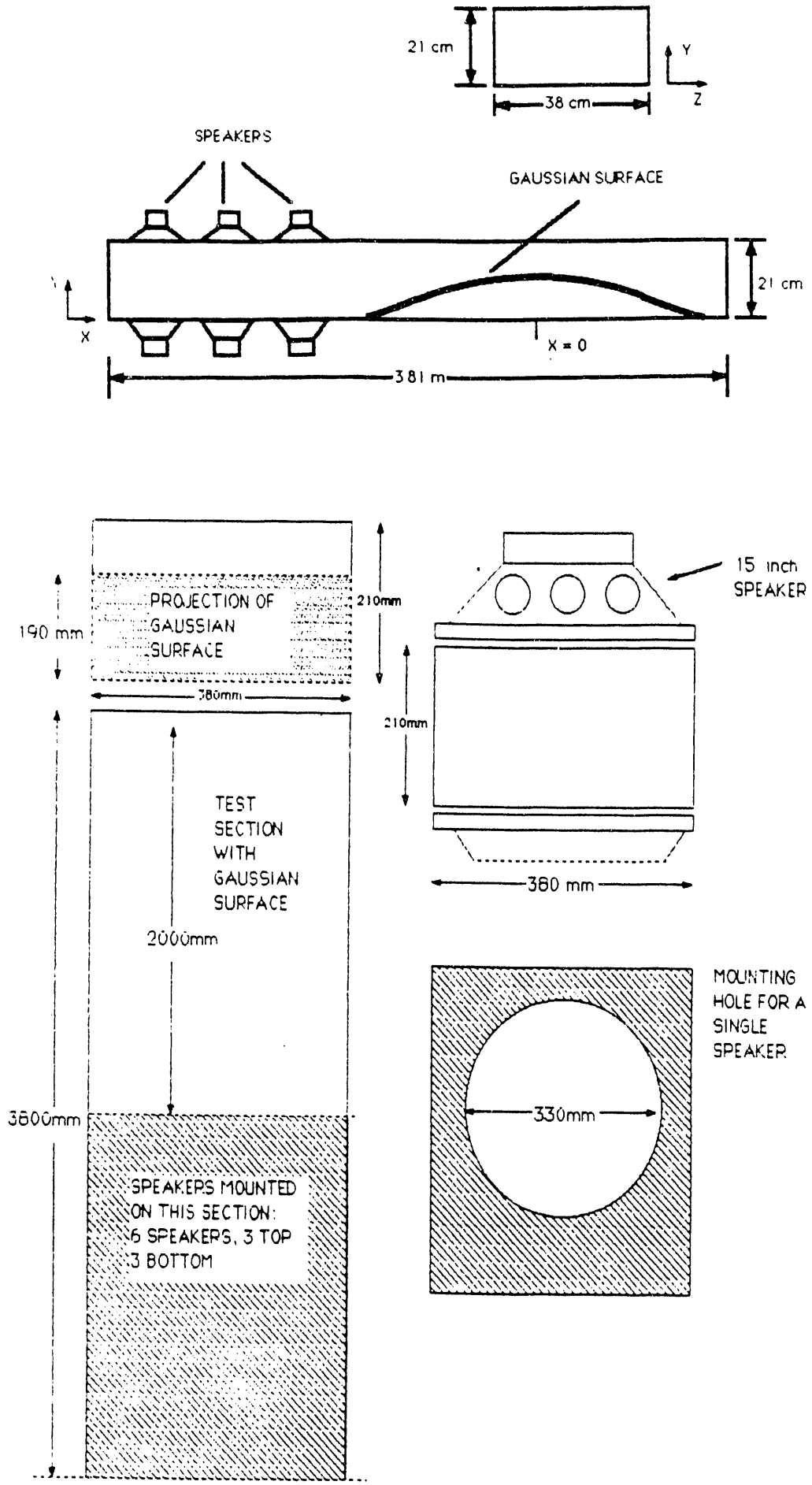

Figure 2.5.1 Schematic of experimental apparatus

Weather stripping is applied on the faces of these panels to eliminate gaps.

The fluid in the channel is driven into harmonic motion by means of six 15*in.* audio speakers. Using speakers as the driving source affords ease in adjusting the frequency and amplitude of the fluid oscillations. The speakers are positioned over symmetrically cut holes along the top and bottom walls of the channel. Leaks were eliminated by applying weather stripping between the outer perimeter of the speaker and the channel walls. A sinusoidal signal from a Krohn–Hite 5100A function generator amplified by a Techron 5530 power supply amplifier is used to drive the speakers. Flow velocity measurements are made using a TSI constant temperature anemometer (Model 1053B) and a TSI hot film probe (Model 1232). A static calibration of the hot film was performed. The offset, exponent, and gain were obtained from the calibration data using a power law relation between the voltage and velocity amplitude.

During an experiment the anemometer signal is stored and processed using a Masscomp 5550 data acquisition computer. Two analog input channels are used. The first channel is used to sample the

anemometer signal and the second channel is used to sample the synchronization signal from the function generator. The rising edge of the synchronization signal is used to trigger the start of the data acquisition process. This signal provides an accurate means for estimating the driving frequency. For a given sample rate, the number of samples taken over a period corresponds to that between two consecutive rising edges. An average of this value is taken over typically five cycles. Since the sampling frequency is known, the source frequency is simply the sampling frequency divided by the average number of samples per period.

The results for the axial velocity for two excitation amplitudes for the frequency of 3.8 Hz are presented in Figures 2.5.2 and 2.5.3. These measurements have been made at $x = 10\ cm$ and $z = 0$, where $x = 0$ corresponds to the zenith of the gaussian boundary. The position $z = 0$ is at the midpoint of the spanwise width. Figure 2.5.2(a) shows one time cycle of the total velocity in the streamwise direction, at five vertical positions. The zero position line is plotted for reference. The velocity signal shows a single maxima during the later half cycle. Because the hot film sensor lies in the wake of the probe support during the first half of the

cycle we see no signal. From this measurement we compute the boundary layer thickness to be approximately 3 mm and a peak velocity of about 1 m/s. The laminar boundary layer thickness is approximately equal to $(2\nu/\omega)^{1/2}$, which corresponds to $1.6mm$. The value of $T(x{=}10cm)$ for this case is equal to 1. The velocity signal exhibits small perturbations superposed on an average profile during the later half of the cycle. These perturbations can be extracted by subtracting the velocity waveform averaged over fifty cycles from the instantaneous signal. The difference signal is shown in Figure 2.5.2(b). The perturbations are small in magnitude, with an amplitude of 8 cm/s and are the result of the electrical noise from the anemometer. This noise appears as a constant fraction of the velocity signal and is independent of location in the boundary layer. Hence, the flow is laminar.

The flow exhibits higher amplitude oscillations when the excitation level is increased. Results for this case are shown in Figure 2.5.3(a). The boundary layer thickness in this case is about 5 mm with a peak velocity amplitude of approximately 3 m/s. This corresponds to local $T(x{=}10cm)$ value of $(9)^{1/2}$ or the edge of the unstable regime. At $x{=}0$ T is equal to

$(20)^{1/2}$. The variations superimposed on the velocity signal decay away from the boundary. The difference signal is given in Figure 2.5.3(b). The velocity variations are again greatest during the second half of the cycle. We also note that these variations subside as we move away from the boundary. The velocity perturbations reach amplitudes of up to $0.4 m/s$.

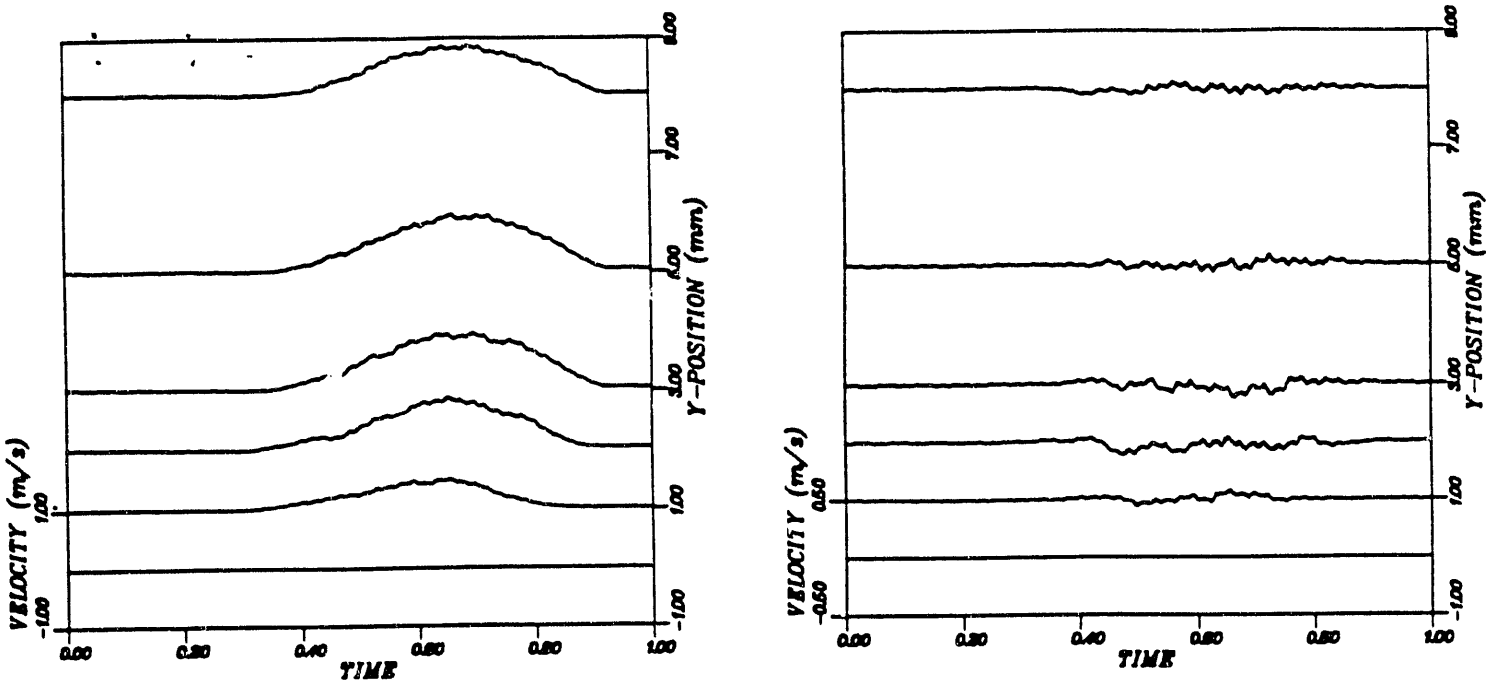

(a) total streamwise velocity

(b) perturbation velocity = (total − average) velocity

Figure 2.5.2 Streamwise velocity measurements. T = 1

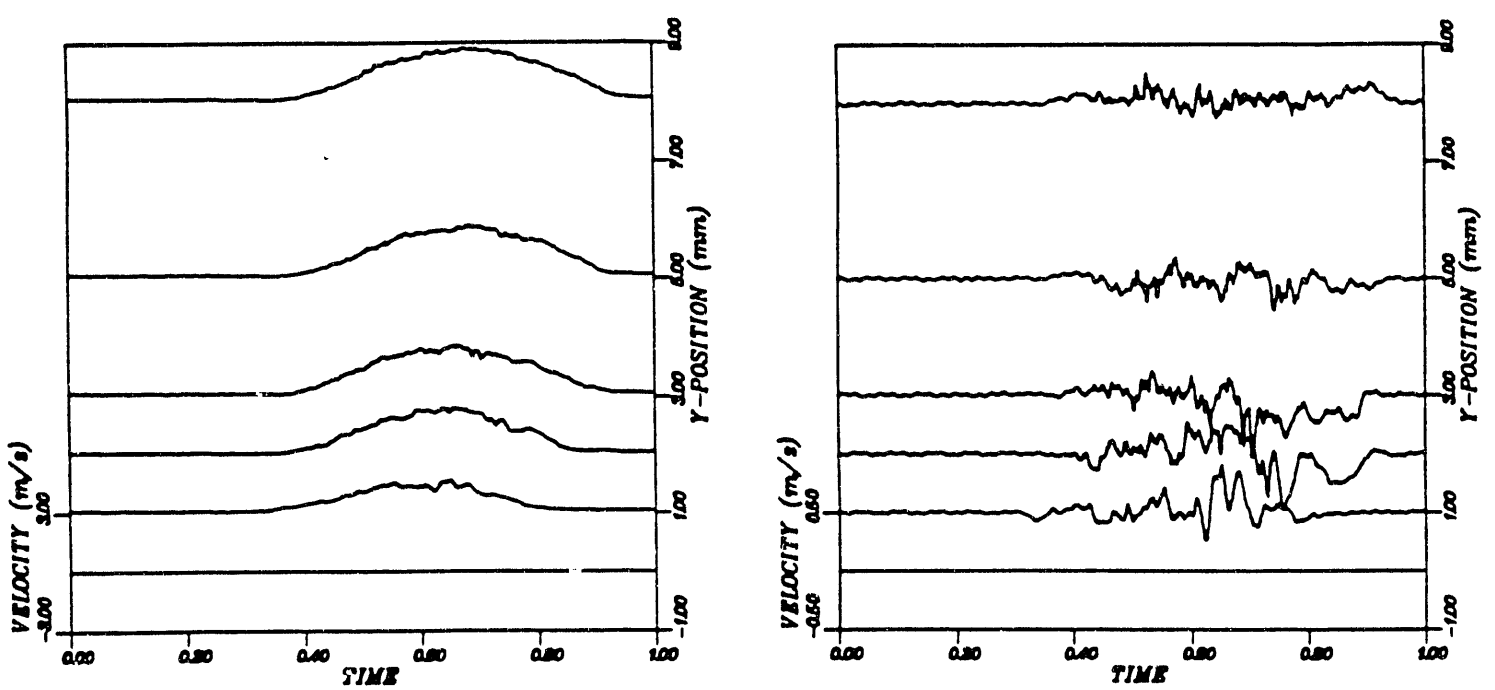

(a) total streamwise velocity

(b) perturbation velocity = (total − average) velocity

Figure 2.5.3 Streamwise velocity measurements. T = $(9)^{1/2}$

References

1. G. G. Stokes, On the effect of the inertial friction of fluids on the motion of pendulums, Cambr. Phil. Trans. IX, 8 (1851); Math. and Phys. Papers, III, 1–141, Cambridge (1901)

2. Lord Rayleigh, On the motion of solid bodies through viscous liquids, Phil Mag., vol 21, 697–711 (1911); Sci. Papers, VI, 29.

2. C. Von Kercek and S. H. Davis, Linear stability theory of oscillatory Stokes layers, J. Fluid Mech., vol. 62, 753 (1974)

3. P. Hall, The linear stability theory of flat Stokes layers, Proc. R. Soc. Lond., A 359, 151 (1978)

4. R. Akahavan, R. D. Kamm and A. H. Shapiro, An investigation of transition to turbulence in bounded oscillatory Stokes flows, J. Fluid Mech., vol. 225, 423 (1991)

5. P. Hall, On the stability of unsteady boundary layer on a cylinder oscillating transversely in a viscous fluid, J. Fluid Mech., vol. 148, 347 (1984)

6. H. Honji, Streaked flow around oscillating an circular cylinder, J. Fluid Mech., vol. 124, 475 (1981)

7. T. Sarpkaya, Force on a circular cylinder in viscous oscillatory flow at low Keulegan–Carpenter numbers, J. Fluid Mech., vol. 165, 61 (1986)

8. C. Thompson, Acoustic streaming in a waveguide with slowly varying height, J. Acoust. Soc. Am., vol. 75, 97 (1984)

9. C. Thompson, Stability analysis of a Stokes boundary layer, J. Acoust. Soc. Am., vol. 81, 861, (1987).

10. C. Thompson, A. Mulpur, V. Mehta and K. Chandra, Transition to chaos in acoustically driven flows, J. Acoust. Soc. Am., vol. 90, 2097 (1991)

11. C. Thompson, V. Mehta, A. Mulpur and K. Chandra Transition to Chaos in Time–Modulated Flow, Proceedings of the 10th Symposium on Energy Engineering Sciences, Argonne, IL., 11–13 May 1992, DOE CONF–9205147

12. C. Thompson, V. Mehta and A. Mulpur, Secondary instability of a Stokes boundary layer, J. Acoust. Soc. Am., vol. 91, p. 2352, (1992)

13. A. Mulpur, V. Mehta, and C. Thompson, Chaotic secondary motions in a oscillatory boundary layer Presented at the 45th Meeting of the American Physical Society, Division of Fluid Mechanics, Tallahassee, FL, Nov 22–24, 1992

15. C. Thompson and V. Mehta Spatial evolution of unstable disturbances in a Stokes boundary layer, J. Acoust. Soc. Am., vol. 91, p. 2352, (1992)

15. V. Mehta, A. Mulpur, and C. Thompson, Spatial evolution of unstable disturbances in a Stokes boundary layer, Presented at the 45th Meeting of the American Physical Society, Division of Fluid Mechanics, Tallahassee, FL, Nov 22–24, (1992)

16. L. Sirovich, Turbulence and the dynamics of coherent structures Part I: Coherent Structures, Q. Appl. Math. XLV, p 561, (1987)

17. K. Chandra, A. Kalkan, C. Thompson, Characterization of structures in chaotic unsteady flows, J. Acoust. Soc. Am., vol. 91, p 2351, (1992)

18. M. J. Lighthill, On sound generated aerodynamically. I The general theory Proc. Roy. Soc. (London) vol. A211, p 564 (1952)

19. R. H. Kraichnan, The scattering of sound in a turbulent medium, J. Acoust. Soc. Am. vol. 25, p 1096 (1953)

20. K. Chandra and C. Thompson, Improved perturbation method for scattering from a fluid cylinder, J. Acoust. Soc. Am. vol. 92, p 1047 (1992)

21. K. Chandra and C. Thompson, Wave propagation in inhomogeneous fluids, Presented at the 45th Meeting of the American Physical Society, Division of Fluid Mechanics, Tallahassee, FL, Nov 22–24, (1992)

END

DATE FILMED

2 / 22 / 93